Journal of Renewable Materials

Tech Science Press

DOI: 10.32604/jrm.2024.055602

ARTICLE

Optimization of Phosphate Adsorption Using Activated Carbon Derived from *Pangium edule* Shell

Rachmannu Ilham[1], Fataty Kurnia Rahmah[1], Nurul Faradilah Said[2], Mohamad Buang Budiono[2] and Suprapto Suprapto[1,*]

[1]Chemistry Department, Faculty of Science and Analytical Data, Institut Teknologi Sepuluh Nopember Surabaya, Surabaya, 60111, Indonesia

[2]Laboratory of Energy and Environment, Institut Teknologi Sepuluh Nopember Surabaya, Surabaya, 60111, Indonesia

[*]Corresponding Author: Suprapto Suprapto. Email: suprapto@chem.its.ac.id

Received: 02 July 2024 Accepted: 03 September 2024 Published: 22 November 2024

ABSTRACT

This study investigated the efficiency of activated carbon from *Pangium edule* shells for removing phosphate from aqueous solution. The adsorption capacity of the synthesized activated carbon was determined to be 19.8392 mg g^{-1}. Various isotherm models were used to analyze the adsorption process, Henry, Freundlich, SIP, and Halsey isotherm fitting showed r^2 values close to 1.0. These isotherms indicated a combination of physisorption and chemisorption mechanisms, with heterogeneity and multilayer formation playing important roles. A pseudo-second-order model described the adsorption kinetics well, suggesting chemisorption as the dominant mechanism with an r^2 value of 1.0 and a rate constant k_2 of 1.2550 min^{-1}. The optimization was carried out using central composite design (CCD) using 3 factors (contact time (minutes), adsorbent dosage (mg), and initial phosphate concentration (ppm)) with 3 levels. The CCD output was analyzed using response surface methodology (RSM) to obtain the optimum level of each factor. A contact time of one to two hours and an adsorbent dosage of more than 80 mg was recommended. Optimal removal was achieved at initial phosphate concentrations between 800 and 1150 ppm. Morphological analysis using scanning electron microscope (SEM) showed a highly irregular surface structure of activated carbon, while X-ray Diffraction (XRD) patterns indicated the presence of amorphous carbon. Fourier Transform Infrared (FTIR) analysis identified functional groups contributing to the adsorption process and Energy Dispersive X-ray Spectroscopy (EDX) analysis confirmed the presence of phosphate on the carbon surface after adsorption. In conclusion, activated carbon from *P. edule* shells has significant potential in phosphate removal, with a combination of high adsorption capacity, effective adsorption mechanism, and favorable kinetics, making it a promising material for water treatment.

KEYWORDS

Adsorption; *Pangium edule*; football fruit; phosphate; Box-Behnken design; response surface methodology

1 Introduction

Phosphate is an important plant nutrient that plays a crucial role in plant growth and aquatic ecosystems. The extensive use of phosphates in agricultural fertilizers has significantly increased crop productivity. However, excess phosphate dissolved into water bodies through agricultural wastewater can cause serious

environmental problems such as eutrophication, which is characterized by excessive algal growth and deterioration of water quality [1]. The problem of phosphate pollution is of global concern due to its harmful effects on aquatic ecosystems and water quality. Eutrophication can lead to hypoxia or oxygen deficiency in water bodies, resulting in mass mortality of aquatic organisms. Therefore, effective methods are needed to reduce phosphate concentration in water bodies to maintain ecosystem balance and environmental health [2,3].

A widely used method to remove phosphate from water is adsorption. This method is considered effective due to its ability to bind phosphate to the surface of the adsorbent, thus enabling efficient separation from water. Adsorption is also flexible and can be used in a wide variety of operating conditions [4]. Recent studies on phosphate adsorption have investigated various materials, including starch-stabilized ferromanganese binary oxide [5], N-Mg doped biochars, La-MOFs, nitrogen-doped activated carbon composites, La and Zr dual-metal modified materials, humic acid coated ferrihydrite, and ZnAlLa ternary layered double hydroxides. Additionally, $La_2(CO_3)_3$-loaded resin for semi-fluidized columns and magnetic field-assisted adsorption on biochar with amorphous Zr-Ce (carbonate) oxide composites have shown promising results for practical applications [6–8]. Advanced materials such as lanthanum hydroxide and lanthanum-modified zeolite have demonstrated stable phosphate adsorption properties in complex water environments [6]. Magnetic biochar with Mg/La modification revealed high effectiveness for phosphate adsorption [9,10]. Other materials explored include hierarchical $ZnO/ZnFe_2O_4$ yolk-shell adsorbents, oxalate-modified nano zero-valent iron, and cellulose fiber impregnated by La/UiO_{66}-NH_2 [11–13].

However, the cost of and preparation of the above materials can be expensive and complicated, limiting its widespread use. To overcome these limitations, several studies have focused on producing activated carbon from low-cost renewable materials and addressing environmental issues by reducing waste production [14,15]. Activated carbon is one of the most commonly used adsorbents due to its large surface area, high porosity, and good adsorption capacity. Processes. Carbonization and activation processes can produce activated carbon from various organic raw materials [16–18]. Activated carbon has been proven effective in removing various pollutants from water, including heavy metals and organic compounds. Much research has been done to develop activated carbon from organic waste to promote sustainability and reduce waste. Using waste as a raw material source reduces the amount of waste to be processed and provides a cheaper and more environmentally friendly alternative raw material for activated carbon production [19–22]. Football Fruit (*Pangium edule*) is known as kluwek in Java, Indonesia. *P. edule* shells, which are wastes of *P. edule* seeds, are potential raw materials for the production of activated carbon. *P. edule* shells have a carbon-rich chemical composition and are available in large quantities as a byproduct of the food industry. Research on the use of *P. edule* shells for activated carbon is still limited, so this study can significantly contribute to this field. Previous research has shown that various types of organic wastes, such as coconut shells and rice husks, can be processed into activated carbon that effectively adsorbs phosphate. The results of this research demonstrate the great potential of organic wastes as a source of activated carbon raw materials, but not many have specifically addressed *P. edule* shells [23,24].

This study introduces a significant innovation by using NaOH-derived activated carbon extracted from football fruit, an underutilized biomass. This approach not only improves the sustainability of carbon utilization but also offers unique properties that can enhance adsorption efficiency. The use of activated carbon derived from football fruit represents an innovative application of agricultural waste and offers potential advantages over traditional materials. Furthermore, the application of response surface methodology (RSM) with Box-Behnken design (BBD) to optimize the adsorption conditions of phosphate ions allows for a systematic and comprehensive analysis of multiple variables, leading to the determination of optimal conditions and interaction between variables for maximum adsorption efficiency.

This combination of a novel carbon source and advanced optimization techniques provides new insights into effective phosphate removal and contributes to the development of more sustainable water treatment technologies [25,26]. This research aims to develop and evaluate the effectiveness of activated carbon made from *P. edule* shells in adsorbing phosphate from water. In particular, this research will characterize the activated carbon produced, test the phosphate adsorption capacity, and determine optimal operating conditions. The results of this research are expected to provide environmentally friendly and economical solutions for water treatment and more effective use of *P. edule* waste.

2 Experimental Section

2.1 Research Design

This research uses the Response Surface Methodology (RSM) method with a Box-Behnken design to optimize the phosphate adsorption parameters using *P. edule* activated carbon. The input factors used in this study were time (minutes), activated carbon dose (mg), and initial phosphate concentration (ppm). The materials used in this research include activated carbon from *P. edule* shells, phosphate solutions with initial concentrations of 200, 400, and 600 ppm, molybdate-vanadate reagent for phosphate measurement, and Aqua demineralization. The instruments used in this research include a UV-Vis spectrophotometer, magnetic stirrer, volume pipette, 100 ml beaker, timer, and analytical balance [27].

2.2 Activated Carbon Preparation

P. edule seed shells were washed and air-dried. The dried seed shells were ground and sieved with a particle size of 100–60 mesh. The *P. edule* seed shell powder was oven-dried until constant weight. *P. edule* seed shells of 100 g were mixed with NaOH solution (with a weight ratio of 1:1) by stirring continuously and left to soak for 3 h. The excess liquid was poured off and the mixture was dried again in an oven at a temperature of 100°C. The mixture was carbonated at 700°C in a nitrogen atmosphere for 2 h. The activated carbon obtained was cooled and then washed with distilled water until the pH was neutral. Finally, the washed activated carbon was dried at a temperature of about 100°C until its weight was constant [16,28,29].

2.3 Preparation of Phosphate Solution

Phosphate solutions with 200, 400, and 600 ppm initial concentrations were prepared by dissolving sodium dihydrogen phosphate (NaH_2PO_4) in distilled water. The solution volume used for each experiment was 100 mL.

2.4 Adsorption Procedure

The Box-Behnken design is used to determine the combination of input factors tested. The three factors tested were time (60, 90, 120 min), activated carbon dose (10, 25, 50 mg), and initial phosphate concentration (200, 400, 600 ppm). A 100 ml of the prepared phosphate solution with the initial concentration, an amount of activated carbon equal to the specified dose is added. The mixture was stirred with a magnetic stirrer at a constant speed. The contact time was determined according to the experimental setup (60, 90, 120 min). After reaching the contact time, the solution is filtered to separate the activated carbon from the solution.

The phosphate concentration in the solution after the adsorption process was measured using the vanadate-molybdate method with a UV-Vis spectrophotometer. Vanadate reagent was prepared by dissolving 1.25 grams of ammonium metavanadate (NH_4VO_3) in 300 ml of hot water. After dissolving, allow the solution to cool and add 330 mL of 65% nitric acid (HNO_3). This solution is then diluted with water to reach a volume of 500 mL. The molybdate reagent was prepared by dissolving 25 grams of ammonium molybdate ($(NH_4)_6Mo_7O_{24}{\cdot}4H_2O$) in 300 mL of water. Add 330 mL of 65% nitric acid (HNO_3) and dilute until a volume of 500 mL is reached. The working reagent was prepared by mixing

1 volume of vanadate solution with 1 volume of molybdate solution. This mixture should be used within 24 h [27,30].

The data obtained were analyzed using the Response Surface Methodology (RSM) to determine the effect of each factor and the interactions between factors on the phosphate adsorption efficiency. The analyses were performed using statistical software that supports Box-Behnken designs. This analysis aims to find optimal operating conditions that maximize the phosphate adsorption capacity. From the results of the RSM analysis, a mathematical model is derived that describes the relationship between input and response factors (phosphate adsorption capacity). Using this model, the optimal conditions for the factors under study are determined. Validation is carried out by conducting experiments under optimal conditions resulting from the model [31,32].

3 Results and Discussion

3.1 Characterization

3.1.1 BET (Brunauer-Emmett-Teller) Analysis

The N_2 adsorption/desorption isotherms of activated carbon (AC) from *P. edule* shells are shown in Fig. 1. The isotherms show the characteristics of Type I and Type IV according to the IUPAC classification, indicating the presence of microporous and mesoporous structures. Type I isotherms are usually associated with microporous materials with relatively small outer areas, while the slight increase in N_2 adsorption at relatively higher pressures suggests the presence of some mesopores inside the AC. The average pore radius of 0.9961 nm and the surface area of 534.952 m^2/g were determined from the BET isotherm analysis. The BJH pore size distribution adsorption results show that the adsorbent surface area was 0.853145 m^2/g with a pore volume of 0.000717166 cc/g, and pore radius, Dv (r), of 1.61665 nm, Table 1. The hysteresis loops observed in the desorption isotherms indicate the presence of gap-shaped micropores and mesopores inside the structure. The *P. edule* shells were carbonized and activated at 700°C [33,34].

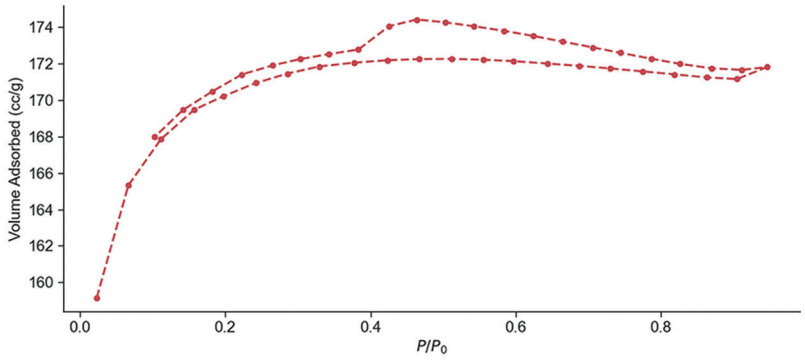

Figure 1: The *P. edule* activated carbon BET isotherm analysis

Table 1: BJH pore size distribution adsorption results

Radius (nm)	Pore volume (cc/g)	Pore surf. area (m^2/g)
1.78741	6.80E-04	8.15E-01
1.97965	7.17E-04	8.53E-01
2.20096	7.17E-04	8.53E-01

(Continued)

Table 1 (continued)

Radius (nm)	Pore volume (cc/g)	Pore surf. area (m^2/g)
2.45651	7.17E-04	8.53E-01
2.77577	7.17E-04	8.53E-01
3.17923	7.17E-04	8.53E-01
3.67001	7.17E-04	8.53E-01
4.33735	7.17E-04	8.53E-01
5.29835	7.17E-04	8.53E-01
6.76971	7.17E-04	8.53E-01
9.29877	7.17E-04	8.53E-01

3.1.2 FTIR

FTIR analysis was performed to identify functional groups present in *P. edule* carbon. Fig. 2 shows the FTIR spectrum of activated carbon obtained from *P. edule* shell. The peak width of about 3422 cm^{-1} is due to the vibration of O–H group, indicating the presence of water molecules. The small shoulder at 2924 cm^{-1} is related to the aliphatic C–H stretching vibration of CH, CH_2, and CH_3 groups. The peak at 2345 cm^{-1} is due to the presence of C≡C group, while the peak at 2085 cm^{-1} is due to the C≡N stretching vibration. The peak at 1622 cm^{-1} is related to the C=O stretching vibration of carboxylic acid. The band at 1444 cm^{-1} is assigned to the asymmetric and symmetric C–H bending vibrations. In addition, a weak band between 900 and 1300 cm^{-1} may indicate the presence of C–O groups in the sample. These variations in functional groups cause activated carbon to have different affinities for different types of molecules, which determines the adsorption properties to target specific pollutants or compounds in specific applications [28,35].

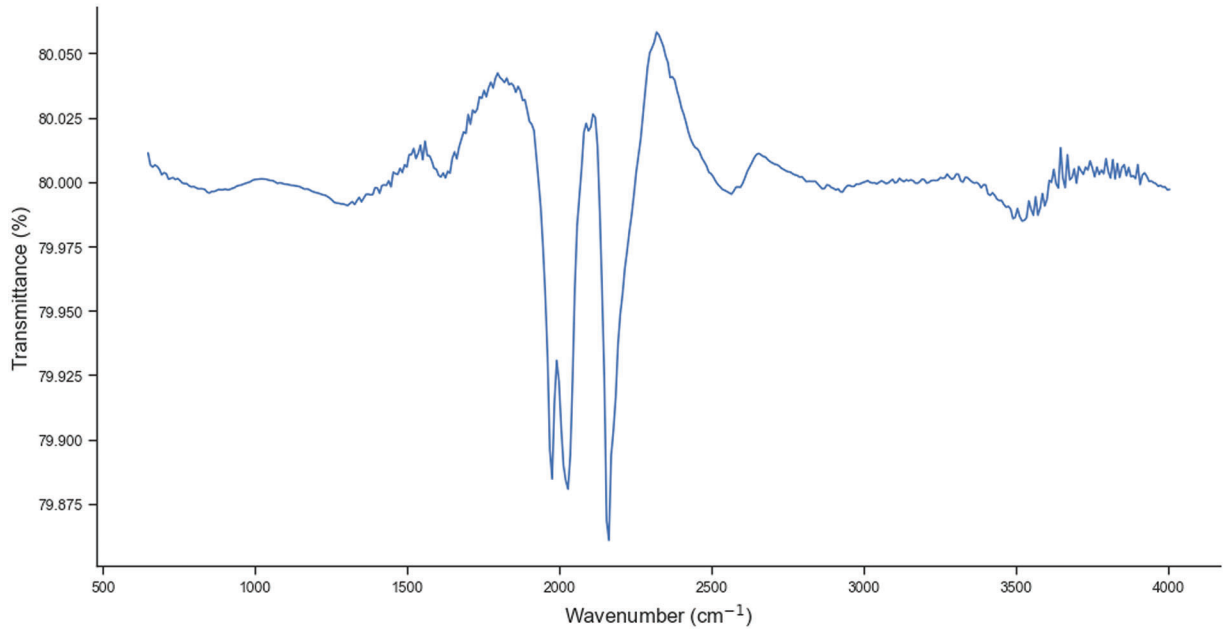

Figure 2: FTIR spectra of *P. edule* activated carbon

3.1.3 SEM-EDX and XRD Analysis

The morphological structure of activated carbon from *P. edule* shell was analyzed by SEM. The SEM image (Fig. 3) shows that the outer surface of activated carbon is very irregular and has various shapes and sizes. This irregularity is most likely due to the release of volatile substances during the carbonization process. In addition, EDX analysis after phosphate adsorption confirmed the presence of phosphate on the surface of *P. edule* carbon, as shown in Fig. 4. The XRD pattern of *P. edule* carbon (Fig. 5) indicates the presence of amorphous carbon.

(a) (b) (c)

Figure 3: The *P. edule* carbon observed at (a) 500, (b) 1000, and (c) 10,000 magnifications

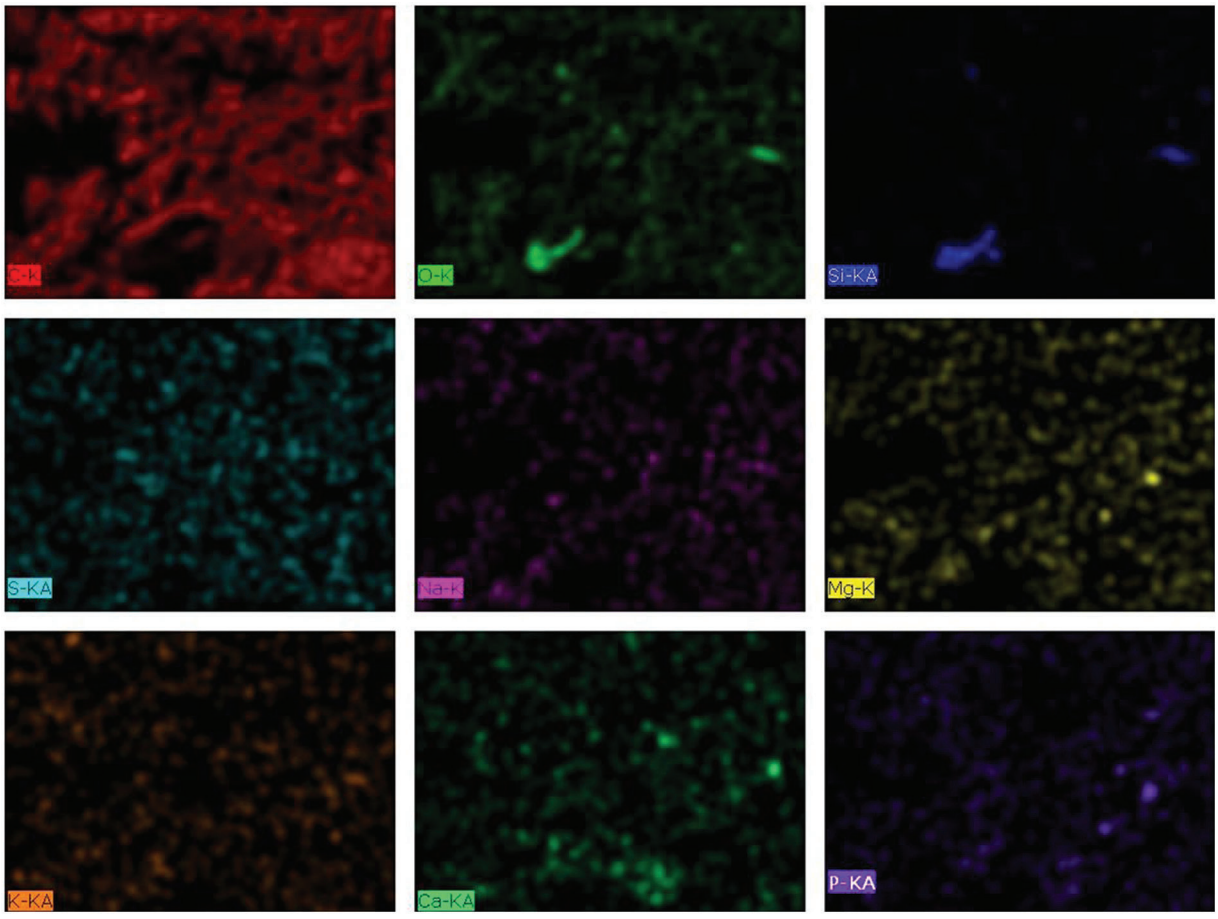

Figure 4: The EDX analysis of *P. edule* carbon after adsorption

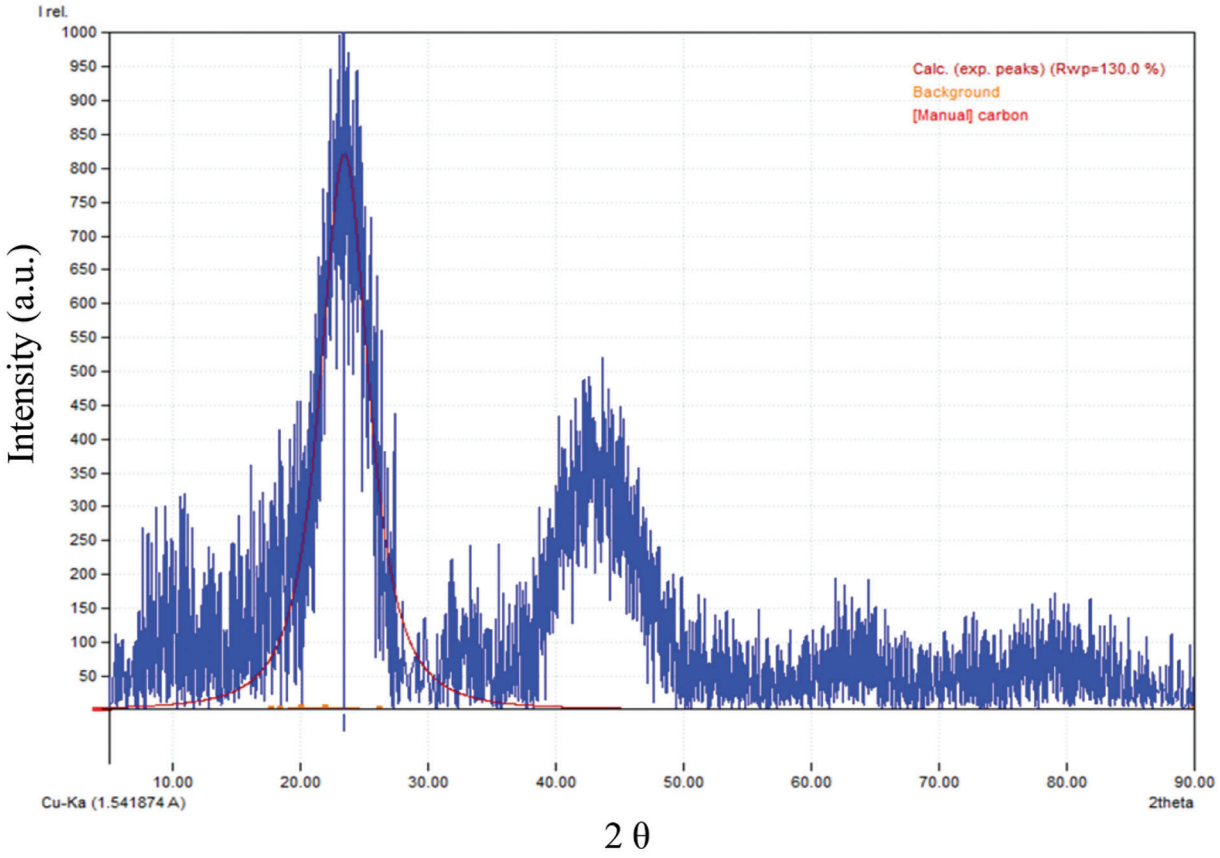

Figure 5: The *P. edule* carbon XRD diffractogram

The X-ray diffractogram of the obtained activated carbon material, Fig. 5, confirmed that the material is composed of three main clusters of atomic planes. The first cluster has a 2θ range of about 5°–15° with a maximum intensity of about 200 a.u. at the second cluster shows a 2θ range of about 20°–25° with a maximum intensity of about 1000 a.u. and the third cluster has a 2θ range of about 35°–50° with a maximum intensity of about 500 a.u. The intensity of these peaks indicates the relative abundance of the atomic clusters, with higher intensity indicating a larger number of atoms. According to Bragg's law, each 2θ value represents the distance between parallel atomic planes (d_hkl) in the hkl-Miller index family. The first cluster (2θ: 5°–15°) has a plane distance of 17.65 to 5.90 Å. The second cluster (2θ: 20°–25°) has an interplanar distance of 4.44 to 3.57 Å. The third cluster (2θ: 35°–50°) has an interplanar distance of 2.56 to 1.82 Å. The results indicate that the nanostructure of processed activated carbon molecules has different interplane distances of parallel atoms, ranging from 17.65 to 1.82 Å. The densest atomic population is in the 2θ region at 20°–25°, followed by the 35°–50° region. The large d-spacing in the first cluster indicates a large amount of amorphous carbon, which is common in activated carbon due to its porous nature and the presence of various functional groups [35].

3.2 Optimization of Phosphate Adsorption

In this study, the optimal conditions for phosphate adsorption were determined by examining several independent factors, including contact time (min), adsorbent dosage (mg), and initial phosphate concentration (ppm). This was achieved using the Box-Behnken design (BBD) and analyzed using Response Surface Methodology (RSM). The experimental and predicted values for phosphate removal are

shown in Fig. 6a. The regression equation for phosphate removal is given in Eq. (1), and the values of the polynomial regression coefficients are shown in Fig. 6b.

$$Z = 96.2964 + 0.0343\,x_0 - 0.0018\,x_1 + 0.0042\,x_2 - 0.0002\,x_0^2 - 0.00005\,x_0x_1 + 0.000001\,x_0x_2 + 0.00015\,x_1^2 - 0.000004\,x_1x_2 - 0.000002\,x_2^2 \quad (1)$$

where Z is the removal of phosphate (%), x_0 is contact time (minute), x_1 is adsorbent dosage (mg), and x_2 is phosphate initial concentration (ppm).

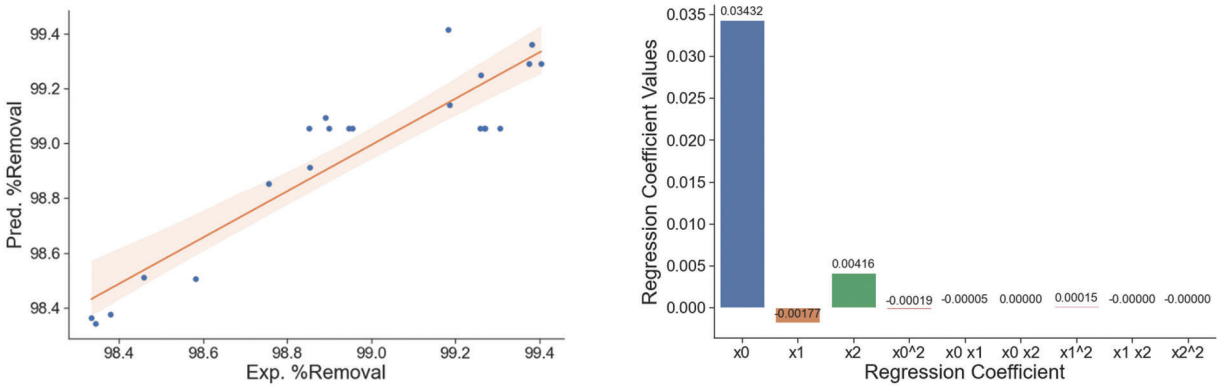

(a) (b)

Figure 6: The regression of experimental and predicted phosphate adsorption (a) and the polynomial regression coefficients of phosphate adsorption (b)

The RSM plot (Fig. 7a–c) shows that contact time significantly affects the removal efficiency, with longer contact time leading to increased phosphate adsorption. The diagram recommends a contact time between one and two hours and an adsorbent dosage of more than 80 mg to achieve optimal adsorption. Considering the interaction between contact time, adsorbent dosage, and initial phosphate concentration, optimal removal was achieved at initial phosphate concentrations between 800 and 1150 ppm.

Based on the polynomial regression model, a phosphate removal efficiency of 99.94% can be achieved with an adsorption time of 86 min, using 50 mg of adsorbent and an initial phosphate concentration of 100 ppm (Fig. 8) [36].

3.3 Adsorption Isotherm

Phosphate adsorption on *P. edule* activated carbon follows the Henry, Freundlich, SIP, and Halsey isotherms. This is supported by the r^2 values of the four isotherms which are close to 1.0 as shown in Fig. 9 and summarized in Fig. 10. At low concentrations, phosphate adsorption follows the Henry isotherm, showing a proportional and direct relationship. This indicates that adsorption is driven by weak forces (physisorption) on a uniform surface [4].

The Freundlich isotherm shows that the surface of activated carbon is heterogeneous and different parts have different affinities for phosphate. This causes different adsorption strengths and means that many phosphate layers can form on the carbon surface.

The SIP isotherm combines features of the Freundlich and Langmuir isotherms. This shows that adsorption at low concentrations resembles the Freundlich isotherm, while at high concentrations it reaches a saturation point. This means that there is a maximum limit to the amount of phosphate that can be adsorbed by coal, this reflects the heterogeneity and limited adsorption capacity.

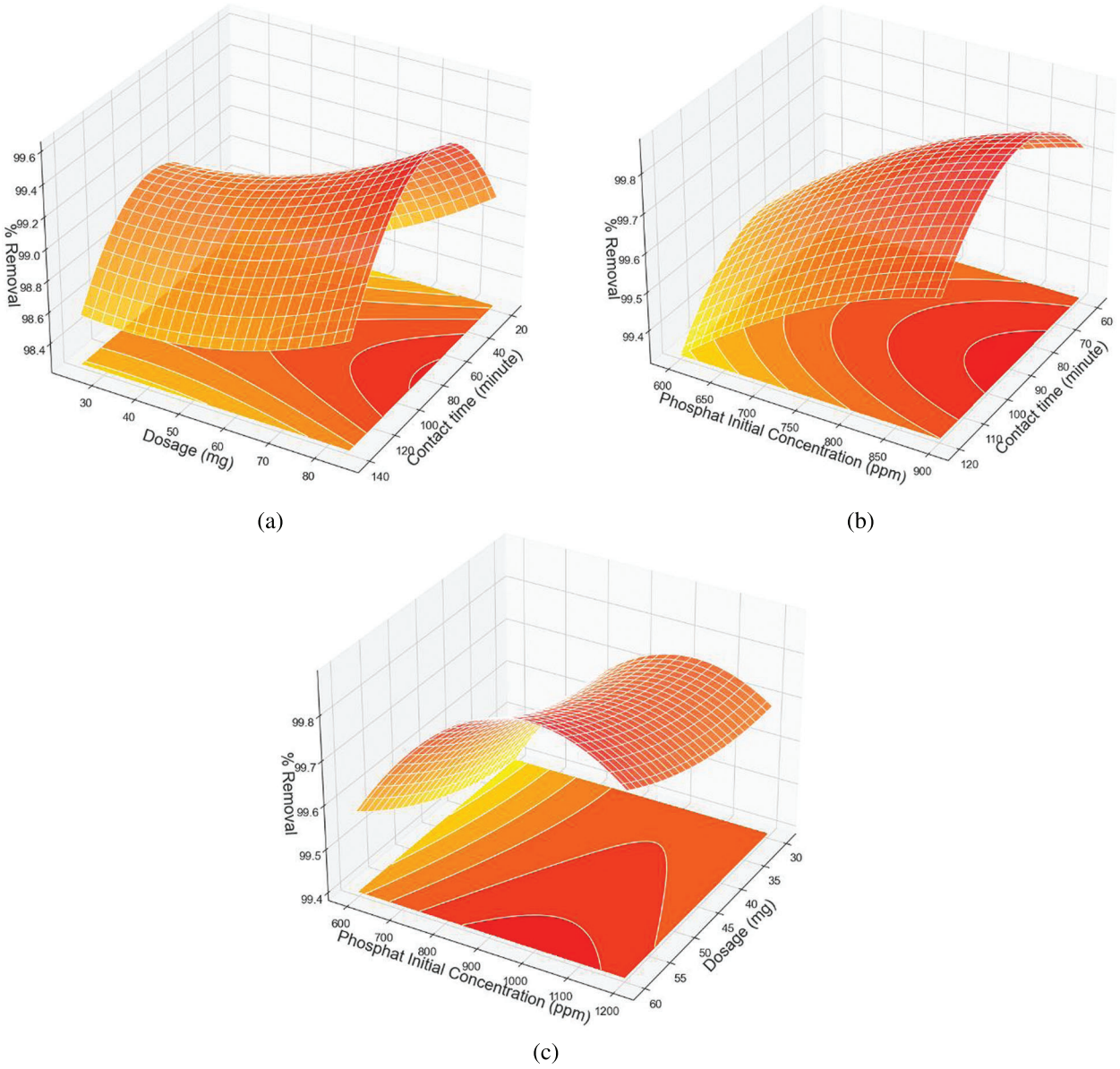

Figure 7: The RSM plot of phosphate adsorption as a function of (a) contact time and adsorbent dosage, (b) contact time and phosphate initial concentration, and (c) adsorbent dosage and phosphate initial concentration

The Halsey isotherm supports the idea that phosphate can form multiple layers on activated carbon, further confirming the heterogeneity of the surface. Overall, phosphate adsorption on activated carbon involves several mechanisms. At low concentrations, weak and uniform physisorption occurs. As the concentration increases, surface heterogeneity becomes apparent, allowing multiple layers to form and saturation point to be reached. Understanding these mechanisms will help optimize the phosphate removal process with *P. edule* activated carbon [33].

Activated carbon obtained from *P. edule* shells has a good phosphate adsorption capacity of 19.8392 mg g^{-1}. This value indicates that the synthesized activated carbon can be effectively used to

remove phosphate from aqueous solutions and other possible water pollutants. The well-developed porous structure, microporosity, and surface chemistry of activated carbon are important factors affecting the adsorption of phosphate on adsorbents [37].

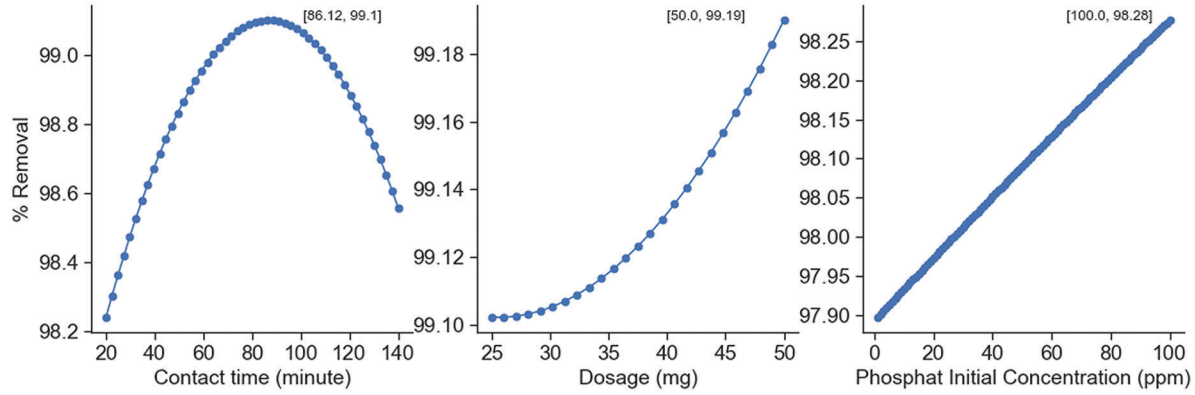

(a) (b) (c)

Figure 8: The optimum phosphate adsorption as a function of (a) contact time, (b) adsorbent dosage, and (c) phosphate initial concentration

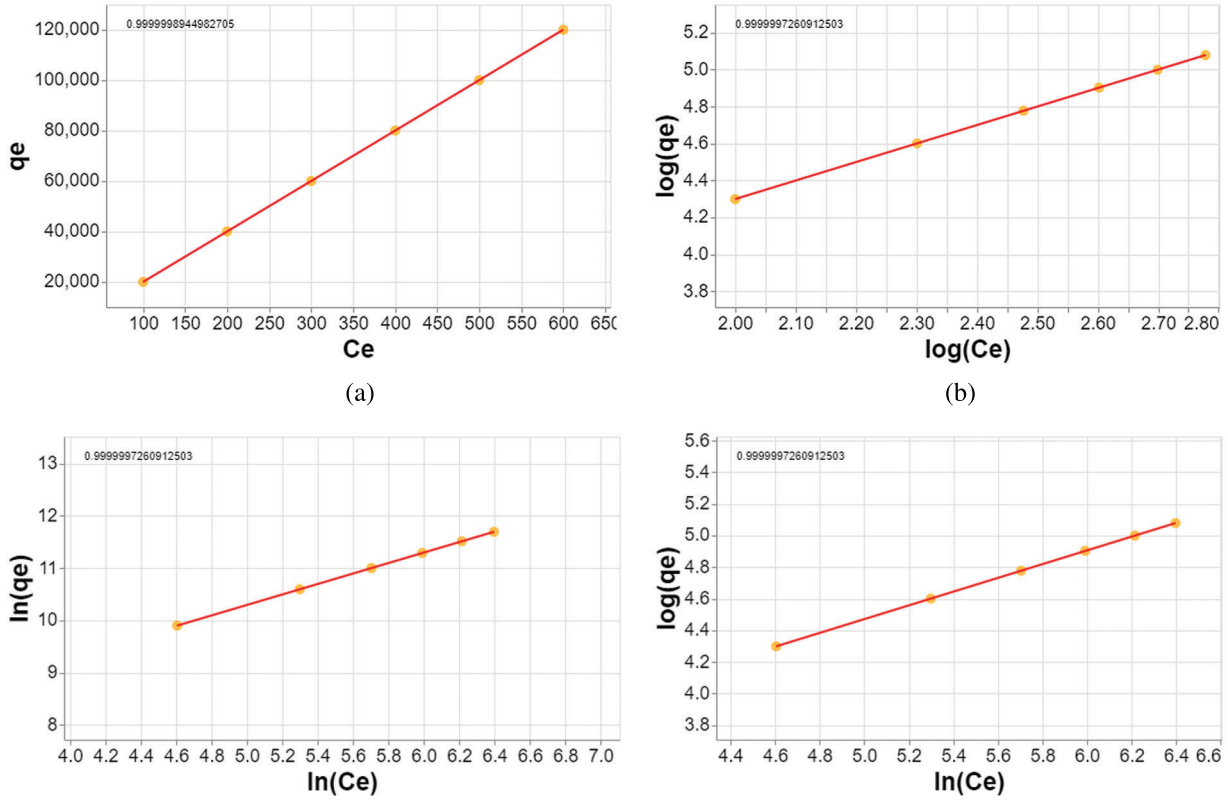

(a) (b) (c) (d)

Figure 9: Fitting the adsorption experimental data into (a) Henry, (b) Freundlich, (c) SIP, and (d) Halsey isotherms

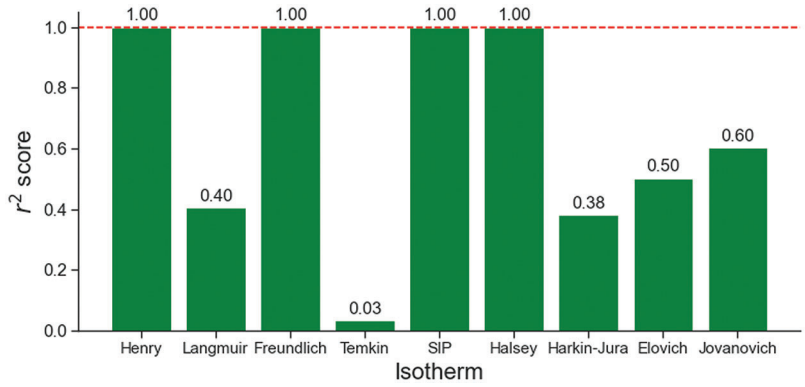

Figure 10: The r^2 score of each adsorption isotherm

3.4 Adsorption Kinetics

Adsorption kinetics is very important to understand the rate and mechanism of adsorption and has direct implications for the efficiency and application of an adsorbent. In this study, the adsorption kinetics are well described by a pseudo-second-order model. The pseudo-second-order equation is represented by Eq. (2).

$$\frac{t}{q_t} = \frac{1}{k_2 q_e{}^2} + \frac{t}{q_e} \tag{2}$$

where q_e is the amount of the phosphate adsorbed at equilibrium (mg/g), q_t is the amount of phosphate adsorbed at t time (mg/g), k_2 is the pseudo-second-order rate constant (minute^{-1}), and t is time (minutes). The pseudo-second-order kinetics model showed a high r^2 value of 1.00 with a k_2 value of 1.255005, as illustrated in Fig. 11. This model indicates that chemisorption is involved in the adsorption process, suggesting that the adsorption mechanism is based on the chemical bonding between the phosphate ions and the active sites on the activated carbon [7,38].

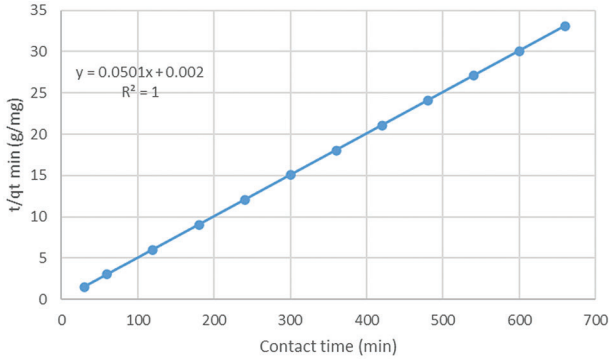

Figure 11: Pseudo-second-order kinetics fitting

4 Conclusion

This study demonstrated that activated carbon from *P. edule* shells effectively removes phosphate from an aqueous solution. The adsorption process was thoroughly analyzed using various isotherms and kinetic models. The activated carbon showed a significant phosphate adsorption capacity of 19.8392 mg g^{-1}, indicating its potential to remove phosphate and other water pollutants. Phosphate adsorption followed Henry, Freundlich, SIP, and Halsey isotherms with high r^2 values approaching 1.0. This suggests the

presence of multiple adsorption mechanisms. At low concentrations, adsorption is driven by weak physisorption on a uniform surface. The heterogeneous surface of activated carbon allows different adsorption strengths and the formation of multiple phosphate layers. The SIP isotherm combines the features of Freundlich and Langmuir isotherms and shows a transition from Freundlich behavior at low concentrations to saturation at high concentrations. The Halsey isotherm supports the formation of multiple layers on heterogeneous surfaces. The adsorption kinetics can be well described by a pseudo-second-order model with an r^2 value of 1.00 and a rate constant k_2 of 1.255005. This indicates that the adsorption process is driven by chemisorption, where chemical bonds occur between phosphate ions and active sites on activated carbon. The optimal conditions for phosphate adsorption were determined using Response Surface Methodology (RSM) and Box-Behnken Design (BBD). This study recommends a contact time of between one and two hours and an adsorbent dosage of more than 80 mg. Optimal removal was achieved at initial phosphate concentrations between 800 and 1150 ppm. SEM images show a highly irregular surface structure, possibly due to the release of volatiles during carbonization. XRD patterns indicate the presence of amorphous carbon, and EDX analysis confirms the presence of phosphate on the carbon surface after adsorption. FTIR analysis identifies various functional groups that contribute to adsorption.

Overall, this study concludes that activated carbon from *P. edule* shells is a promising adsorbent for phosphate removal because it combines high capacity, effective adsorption mechanism, and favorable kinetics. Understanding these factors helps optimize the adsorption process and enhances the practical application of this material in water treatment [12].

Future research on activated carbon from *P. edule* shells can focus on long-term performance testing to evaluate stability and durability over time, and effective regeneration methods should be explored to restore adsorption capacity after phosphate saturation. In addition, extending the study to remove other pollutants such as heavy metals and pharmaceuticals will broaden its application. In order to understand the interaction of phosphate with coal functional groups, in-depth mechanistic studies using techniques such as XPS or HRTEM are needed. Scaling up production and conducting pilot-scale testing will help evaluate performance in practice, while research on functionalization or modification can further improve its adsorption capacity and selectivity.

Acknowledgement: The authors gratefully acknowledge the financial support provided by DRPM, Institut Teknologi Sepuluh Nopember, Surabaya, Indonesia.

Funding Statement: This study was funded by DRPM, Institut Teknologi Sepuluh Nopember, under Research Grant No. 1284/PKS/ITS/2024, dated 29 February 2024.

Author Contributions: Study conception and design: Rachmannu Ilham. Data collection: Fatati Kurnia, Nurul Faradilah Said, Mohamad Buang Budiono. Analysis and interpretation of results: Rachmannu Ilham, Fatati Kurnia, Suprapto Suprapto. Draft manuscript preparation: Rachmannu Ilham, Suprapto Suprapto. Writing—review, and editing: Rachmannu Ilham, Suprapto Suprapto. Supervision: Suprapto Suprapto. All authors reviewed the results and approved the final version of the manuscript.

Availability of Data and Materials: Data will be made available on request.

Ethics Approval: Ethics approval is not applicable for this research as it does not involve human participants, their tissue, or their data.

Conflicts of Interest: The authors declare no conflicts of interest to report regarding the present study.

References

1. Pap S, Zhang H, Bogdan A, Elsby DT, Gibb SW, Bremner B, et al. Pilot-scale phosphate recovery from wastewater to create a fertiliser product: an integrated assessment of adsorbent performance and quality. Water Res. 2023;228:119369. doi:10.1016/j.watres.2022.119369.
2. Douterelo I, Dutilh BE, Calero C, Rosales E, Martin K, Husband S. Impact of phosphate dosing on the microbial ecology of drinking water distribution systems: fieldwork studies in chlorinated networks. Water Res. 2020;187:116416. doi:10.1016/j.watres.2020.116416.
3. Abu-Hilal AH. Phosphate pollution in the Jordan Gulf of Aqaba. Mar Pollut Bull. 1985;16(7):281–5. doi:10.1016/0025-326X(85)90567-3.
4. Zeng J, Chen D, Zhu J, Long C, Qing T, Feng B, et al. Phosphate recovery using activated sludge cyanophycin: adsorption mechanism and utilization as nitrogen-phosphorus fertilizer. Chem Eng J. 2023;476:146607. doi:10.1016/j.cej.2023.146607.
5. Yun J, Shahi NK, Dockko S. Adsorption performance and mechanism of a starch-stabilized ferromanganese binary oxide for the removal of phosphate. Chemosphere. 2024;362:142864. doi:10.1016/j.chemosphere.2024.142864.
6. Zhao M, Zhou X, Li J, Li F, Li X, Yu J, et al. Efficient removal of phosphate and fluoride from phosphogypsum leachate by lanthanum-modified zeolite: synchronous adsorption behavior and mechanism. J Environ Chem Eng. 2024;12(5):113294. doi:10.1016/j.jece.2024.113294.
7. Nazarian R, Desch RJ, Thiel SW. Kinetics and equilibrium adsorption of phosphate on lanthanum oxide supported on activated carbon. Colloids Surf A Physicochem Eng Asp. 2021;624:126813. doi:10.1016/j.colsurfa.2021.126813.
8. Mainali K, Mullen CA, Sarker MI, Haghighi Mood S, Garcia-Perez M. Production of *N*-Mg doped biochars for phosphate adsorption from renewable sources. Biomass Bioenergy. 2024;185:107221. doi:10.1016/j.biombioe.2024.107221.
9. He Q, Zhao H, Li M. Tuning microscopic structure of La-MOFs via ligand engineering effect towards enhancing phosphate adsorption. J Environ Manage. 2024;353:120149. doi:10.1016/j.jenvman.2024.120149.
10. He Y, Feng T, Huang Q, Zhang C, Li G. Nitrogen-doped activated carbon composite electrode for deionization of phosphate removal and DFT model adsorption of phosphates. Chemosphere. 2024;142973. doi:10.1016/j.chemosphere.2024.142973.
11. Hu Y, Li Y, Zhang H. Adsorption and recovery of phosphate using sodium carbonate as co-precipitant synthesized La & Zr dual-metal modified material: adsorption mechanism and practical application. Chemosphere. 2024;363:142878. doi:10.1016/j.chemosphere.2024.142878.
12. Zhang Y, Zheng Z, Badsha MAH, Lo IMC. Advancing phosphate removal: unleashing the adsorption/desorption potential of $La_2(CO_3)_3$-loaded resin by semi-fluidized columns and *in-situ* regeneration. Sep Purif Technol. 2024;341:126835. doi:10.1016/j.seppur.2024.126835.
13. Ren L, Zhang J, Li Y, Zhang C. Preparation and evaluation of cattail fiber-based activated carbon for 2,4-dichlorophenol and 2,4,6-trichlorophenol removal. Chem Eng J. 2011;168(2):553–61. doi:10.1016/j.cej.2011.01.021.
14. Ullah S, Shah SSA, Altaf M, Hossain I, El Sayed ME, Kallel M, et al. Activated carbon derived from biomass for wastewater treatment: synthesis, application and future challenges. J Anal Appl Pyrolysis. 2024;179:106480. doi:10.1016/j.jaap.2024.106480.
15. Subba Reddy Y, Rotte NK, Sudhakar BK, Ramakrishna Chand N, Janraj Naik R, Mandal S, et al. Biomass-derived sustainable mesoporous activated carbon as an efficient and recyclable adsorbent for the adsorption of hazardous dyes. Hybrid Adv. 2024;6:100218. doi:10.1016/j.hybadv.2024.100218.
16. Sharma S, Ezung SL, Supong A, Baruah M, Kumar S, Umdor RS, et al. Activated carbon adsorbent derived from waste biomass, "Croton caudatus" for efficient removal of 2-chlorophenol from aqueous solution: Kinetics, isotherm, thermodynamics and DFT simulation. Chem Eng Res Des. 2023;190:777–92. doi:10.1016/j.cherd.2023.01.002.
17. Hussain A, Maitra J, Saifi A, Ahmed S, Ahmed J, Shrestha NK, et al. A sustainable approach for fluoride treatment using coconut fiber cellulose as an adsorbent. Environ Res. 2024;244:117952. doi:10.1016/j.envres.2023.117952.

18. Aktar MS, Shakil MSR, Tuj-Zohra F. Potentials of bio-adsorbent prepared from coconut fibre in mitigation of pollution from tanning effluent. Cleaner Eng Technol. 2023;17:100687. doi:10.1016/j.clet.2023.100687.
19. Mondal MIH, Chakraborty SC, Rahman MS, Marjuban SMH, Ahmed F, Zhou JL, et al. Adsorbents from rice husk and shrimp shell for effective removal of heavy metals and reactive dyes in water. Environ Pollut. 2024;346:123637. doi:10.1016/j.envpol.2024.123637.
20. Bhatia D, Saroha AK. Biochar derived from pyrolysis of rice straw as an adsorbent for removal of phenol from water. J Water Process Eng. 2024;59:105003. doi:10.1016/j.jwpe.2024.105003.
21. Halim AA, Aziz HA, Johari MAM, Ariffin KS. Comparison study of ammonia and COD adsorption on zeolite, activated carbon and composite materials in landfill leachate treatment. Desalination. 2010;262(1):31–5. doi:10.1016/j.desal.2010.05.036.
22. Ismail M, Khan AM, Naeem A, Rehman Z, Aziz T, Mushtaq K, et al. Levels and potential health hazards of chlorinated pesticides in surface water samples of Charsadda area of Pakistan using SPME-GC-ECD technique. Water. 2021;13(18):2468. doi:10.3390/w13182468.
23. Waluyo R, Hadju A, Rati Y, Marlina R, Darma Y. Facile synthesis of *Pangium edule* kernel biomass-derived NCQDs/TiO_2/PVA nanocomposite film for visible light-assisted methylene blue reduction. Biomass Bioenergy. 2024;180:106992. doi:10.1016/j.biombioe.2023.106992.
24. Astutik S, Pretzsch J, Kimengsi JN, Kapp G. Medicinal plants production systems in rural Indonesia: management practices and performance insights. Forest Policy Econ. 2023;153:102972. doi:10.1016/j.forpol.2023.102972.
25. Yazid H, Grich A, Bahsis L, Regti A, El Himri M, El Haddad M. Exploring and studying the adsorption mechanisms of the herbicides 2,4,5-T and 2,4-D on activated carbon from walnut shells, using theoretical DFT analyses and a central composite design. Results Surf Interfaces. 2024;14:100192. doi:10.1016/j.rsurfi.2024.100192.
26. Almahbashi NMY, Kutty SRM, Jagaba AH, Al-Nini A, Al-Dhawi BNS, Rathnayake U. Phenol removal from aqueous solutions using rice stalk-derived activated carbon: equilibrium, kinetics, and thermodynamics study. Case Stud Chem Environ Eng. 2023;8:100471. doi:10.1016/j.cscee.2023.100471.
27. Shyla B, Mahadevaiah, Nagendrappa G. A simple spectrophotometric method for the determination of phosphate in soil, detergents, water, bone and food samples through the formation of phosphomolybdate complex followed by its reduction with thiourea. Spectrochim Acta A Mol Biomol Spectrosc. 2011;78(1):497–502. doi:10.1016/j.saa.2010.11.017.
28. Shin S, Jang J, Yoon SH, Mochida I. A study on the effect of heat treatment on functional groups of pitch based activated carbon fiber using FTIR. Carbon. 1997;35(12):1739–43. doi:10.1016/S0008-6223(97)00132-2.
29. Zhang Y, Dong X, Liu H, Gao T, Ren Y, Meng Y, et al. A novel approach for predicting the carbon content of birch leaf litter using Fourier transform infrared (FTIR) spectroscopy. Microchem J. 2024;200:110262. doi:10.1016/j.microc.2024.110262.
30. Habibah N, Dhyanaputri IGAS, Karta IW, Sundari CDWH, Hadi MC. A simple spectrophotometric method for the quantitative analysis of phosphate in the water samples. Jurnal Sains dan Teknologi. 2018;7(2). doi:10.23887/jstundiksha.v7i2.13940.
31. Ni'mah YL, Pertiwi AC, Suprapto S. Adsorption of Cu(II) on silica gel synthesized from chemical bottle glass waste: response surface methodology-Box Behnken design optimization. South Afr J Chem Eng. 2024;48:55–62. doi:10.1016/j.sajce.2024.01.007.
32. Ni'mah YL, Suprapto S, Perdana AK, Subandi, Yuningsih NE, Pertiwi AC. The optimization of silica gel synthesis from chemical bottle waste using response surface methodology. Arab J Chem. 2022;15(12):104329. doi:10.1016/j.arabjc.2022.104329.
33. Van Erp TS, Martens JA. A standardization for BET fitting of adsorption isotherms. Microporous Mesoporous Mater. 2011;145(1):188–93. doi:10.1016/j.micromeso.2011.05.022.
34. Joshi N, Romanias MN, Riffault V, Thevenet F. Investigating water adsorption onto natural mineral dust particles: linking DRIFTS experiments and BET theory. Aeolian Res. 2017;27:35–45. doi:10.1016/j.aeolia.2017.06.001.
35. Wibawa PJ, Nur M, Asy'ari M, Nur H. SEM, XRD and FTIR analyses of both ultrasonic and heat generated activated carbon black microstructures. Heliyon. 2020;6(3). doi:10.1016/j.heliyon.2020.e03546.

36. Ni'mah YL, Subandi APK, Suprapto S. The application of silica gel synthesized from chemical bottle waste for zinc (II) adsorption using Response Surface Methodology (RSM). Heliyon. 2022;8(12). doi:10.1016/j.heliyon.2022.e11997.
37. Shan X, Zhu S, Zhang W. Effect of surface modification of activated carbon on its adsorption capacity for NH_3. J China Univ Min Technol. 2008;18(2):261–74. doi:10.1016/S1006-1266(08)60055-3.
38. Yang Z, Sultan M, Shahzad MW, Thu K, Miyazaki T. A comprehensive investigation of R32 adsorption kinetics onto MSC30 activated carbon powder. Int Commun Heat Mass Transfer. 2023;149:107148. doi:10.1016/j.icheatmasstransfer.2023.107148.